Molecular Dynamics Investigation of the Structural and Mechanical Properties of Off-Stoichiometric Epoxy Resins

Chang Woon Jang[1,5,*], Jin Ho Kang[2], Frank L. Palmieri[3], Tyler B. Hudson[3], Charlotte J. Brandenburg[4], John W. Lawson[5,*]

[1]KBR, NASA Ames Research Center, Moffett Field, California 95035, USA

[2]National Institute of Aerospace, Hampton, Virginia 23666, USA

[3]NASA Langley Research Center, Hampton, Virginia, 23681, USA

[4]NASA Langley Student Intern, Iowa State University, Ames, Iowa 50011, USA

[5]Intelligent System Division, NASA Ames Research Center, Moffett Field, California 94035, USA

ABSTRACT: Molecular dynamics (MD) simulations were performed to compute the mechanical properties of off-stoichiometric epoxy resins as a function of hardener/epoxy mixture ratio (r). Properties were characterized in relation to their microscopic structures. Such resins have been used recently for adhesive-free bonding of large-scale composite structures using the co-curing-ply method. In this process, two partially precured composite panels with hardener poor (HP) off-stoichiometric resins are coupled with ply(ies) of complementary hardener rich (HR) formulations and then cured simultaneously. This bonding process has the potential to produce reliable and certifiable composite joints without the need for additional fasteners, which are often required for many conventional bonding methods because even small amounts of contamination can cause a weak bond. The reflow and mixing of the HP/HR resin in this bonding process results in a joint with no discernable interface that should not be susceptible to surface contamination. However, incomplete mixing of the two offset resins may result in chemical heterogeneity of the cured polymeric joint. Thus, different r values may be obtained across the joint. Classical MD simulations were performed to compute the Young's modulus of polymers with different r values and correlate their properties to network structures. High stiffness was associated with molecular packing due to chemical cross-linking, leading to a single network structure. Moreover, the networks became denser as the ratio approached the stochiometric value $r = 1$. Thus, the $r = 1$ systems were single clusters, with high stiffness, high molecular weight, and a high degree of cross-linking. Structural properties such as radius of gyration and mean square displacement were determined to investigate the variation in the stiffness with respect to r. This MD simulation study was validated with experimental measurements.

KEYWORDS: MD Simulations, Mechanical Properties, Off-Stoichiometric Epoxy, Atomistic Structure-Property Relationship, Epoxy Crosslinking

1. INTRODUCTION

Large-scale polymer matrix composites in the aerospace industry are commonly manufactured using epoxy adhesive bonding.[1] Due to the unpredictable nature of composite-adhesive bonding interfaces resulting from conventional bonding techniques, additional redundant mechanical fasteners are commonly used to ensure safety in critical applications and to meet Federal Aviation Administration (FAA) certification criteria for composite structures.[1] Recently, advanced airframe technologies have been developed using reflowable interface bonding to reduce the uncertainty in the structural performance of the composite assemblies, thus reducing the need for redundant fasteners.[2-9] These composite structures offer the potential to achieve more affordable and higher manufacturing rate. In addition, these efficient structures are expected to increase aircraft performance due to the considerable weight reduction. The two-step, co-cure-ply technique recently proposed produces joints with the reliability of the co-cure method. However, this is limited by the complexity of the part and/or the size of the autoclave,[10] with the manufacturability of secondary bonding. With this method, large-scale composite components are bonded using stoichiometric offset resins.[2-9]

The co-cure-ply bonding method, proposed by Palmieri *et al.*[2-9] utilizes two complementary, off-stoichiometric resins, designated as hardener-poor (HP) and hardener-rich (HR). These resins are characterized by a hardener/epoxy ratio *r* defined as the total number of hardener functional groups to the total number of epoxy functional groups:

$$r = \frac{Molar\ Equiv.Hardener}{Molar\ Equiv.Epoxy} = \frac{\sum f_H n_H}{\sum f_E n_E} \tag{1}$$

where f_H and f_E are the number of functionalities and n_H and n_E are the number of monomers of hardener and epoxy molecules, respectively. HR resins have $r > 1$; whereas, HP reins have $r < 1$.

In general, HR and HP resins have complementary r values, where full stoichiometry (r = 1) is recovered when the two resins are completely mixed.

The co-cure-ply bonding method is a two-step cure process. First, the HP resin (often in the form of prepreg) is partially cured during the primary cure step on the mating surface of two composite parts composed of conventional (r = 0.8–1.0) material. Note that off-stochiometric resin surface does not undergo complete conversion during cure. Then, the two composite parts are mated with a layer(s) (i.e., ply(ies)) composed of hardener-rich resin and a structural reinforcement/carrier (often carbon fiber). Both panels are then cured together in a secondary cure step. During the secondary cure, the resin molecules can diffuse between the HR and HP regions. Ideally, complete mixing would be achieved during the secondary cure, resulting in a stochiometric (r = 1), fully cured, homogeneous interfaces. However, resin mobility is reduced due to the heterogeneous molecular sizes produced during the primary cure. Thus, complete mixing between HR and HP resins is typically not achieved due to long diffusion times. Thus, the effective r values will vary across the bonded interface. This stoichiometric variation will result in different local mechanical properties across the interface as shown in Figure 1. At the contact between the two resins, the hardener to epoxy mixture ratio is expected to be close to stoichiometric (r = 1) since mixing should be the highest in the contact region. The stiffness therefore is expected to be highest at this point.

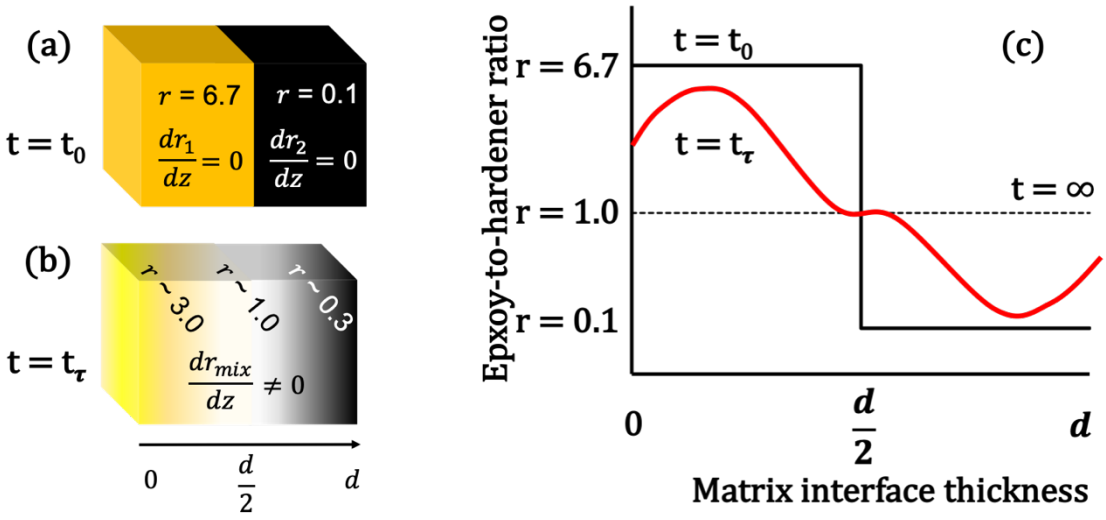

Figure 1. Hardener-to-epoxy ratio *r* distribution for an interface of thickness *d* with complementary offset resins (r = 0.1, r = 6.7) (a) before secondary cure ($t = t_0$) and (b) after ($t = t_\tau$) secondary cure. Time *t* is the duration of the secondary cure. (c) Distribution of *r* values across a heterogeneous interface of thickness *d* before and after the secondary cure. Ideal mixing, i.e. a homogeneous interface, is only achieved for very long mixing times ($t = t_\infty$).

The goal of this study is to investigate the effect of the ratio *r* on the mechanical properties of off-stoichiometric polymer resins. We used molecular dynamics (MD) simulations to investigate structure-property relationships for these systems. MD simulations cannot be performed for macroscale systems due to the limited time and length scales accessible. Therefore, only local nanoscale regions can be considered. We view the bonded joint as discretized into small regions, each domain being considered as homogeneous with respect to *r*. MD simulations were able to investigate various epoxy systems with different *r* values, representing the different domains. MD simulation results such as Young's modulus and Poisson's ratio can then be used to predict the bulk properties of the bonded joint using higher length scale computations like finite

element analysis (FEA). In such a multiscale framework, the constitutive relations are thus obtained from MD at the nanoscale.

In this study, we focused on calculating the elastic mechanical properties of crosslinked amine/epoxy systems as a function of the offset ratio *r* using uniaxial tensile tests. Stiffness values were rationalized by molecular structural analysis such as intra-network connectivity, radius of gyration, and mean squared displacement. This paper is organized as follows. In Section 2, details of the modeling and simulation methods used to generate the crosslinked network are presented. In Sections 3 and 4, the mechanical and structural properties of crosslinked networks of various offset resins are addressed. A subsequent multiscale approach to obtain bulk interfacial material properties of macroscopic epoxy polymer will also be discussed.

2. MOLECULAR MODELS AND SIMULATIONS METHODS

2.1. Epoxy and Hardener Monomers

The API-60 epoxy system modeled in this study is an aerospace-grade epoxy resin and is commercially available from Applied Poleramic Inc. (now Kaneka North America). It is a mixture of two parts. Part A is composed of 60–80% 4,4'-methylenebis (N, N-diglycidylaniline) tetra-functional epoxy (E_4), 10–20 % N, N-diglycidyl-4-glycidyloxyaniline tri-functional epoxy (E_3). The Part A also contains an unknown proprietary toughener that is not included in the simulations. This may cause the discrepancy of mass density between simulations and experiments. Part B is a curing agent hardener, di-amine tetra-functional 4,4'-diaminodiphenyl sulfone. The chemical structures of the epoxy molecules used in this study are appended in Figures *S*1(a) and *S*1(b). These two monomers are designated as TGDDM and TGAP corresponding to the functionalities of $f = 4$ and 3, respectively. The Part B is designated as DDS which has the functionality of $f = 4$ as shown

in Figure *S*1(c). A fixed molar ratio of 80/20 for TGDDM/TGAP was used in this study. The molar ratio of DDS to TGDDM+TGAP varies with the offset ratio *r*.

2.2. Offset Resin Systems and Initial Equilibration

Eight off-stoichiometric resin models were created including three hardener poor systems ($r < 1$), four hardener rich systems ($r > 1$), and a perfect stoichiometric mixture ($r = 1.0$). The total number of molecules and their weight fractions are given with the corresponding *r* value in Table *S1*. For each *r* value, five different initial configurations were created using three-dimensional (3-D) periodic boundary conditions. Molecules were loaded into a cell and arranged in a random fashion using Packmol package.[11]

All simulations were performed using Large-scale Atomic/Molecular Massively Parallel Simulator (LAMMPS)[12] and the second generation of the General Amber Force Field (gaff2) developed by Wang.[13] They refit the first generation of gaff for both the van der Waals interaction energies and the bonded force field parameters using high quality *ab initio* data. This reparameterization improved the transferability of the gaff2 parameters. The gaff2 potential energy includes bonded and non-bonded functional forms and is expressed as follows:

$$V(r) = \sum_{b} k_b(b - b_0)^2 + \sum_{\theta} k_\theta(\theta - \theta_0)^2 + \sum_{d} \frac{k_\varphi}{2}[1 + \cos(n\varphi - \gamma)] + \cdots$$
$$+ \cdots \sum_{i<j} \left[\frac{A_{ij}}{r_{ij}^{12}} - \frac{B_{ij}}{r_{ij}^{6}} + C\frac{q_i q_j}{r_{ij}}\right] \quad (2)$$

Here, the first three terms are bond (b), angle (θ), and dihedral (φ) interactions and the last term represents the van der Waals and electrostatic interactions. The ks are the force constants for each term, the b_0 and θ_0 are the bond and angle equilibrium structural parameters, and n and γ are multiplicity and phase angle parameters for the dihedral angle, respectively.

Initial systems were equilibrated before curing as follows. First, energy minimization was performed using the conjugate gradient method to partially relax the molecules and minimize the total energy of the system. Then, a series of MD simulations were performed using the canonical ensemble NVT (constant number of atoms: N; constant volume, V; and constant temperature, T) and a isobaric-isothermal ensemble NPT (constant number of atoms: N; constant volume, V; and constant pressure, T) at 300 K and 1 atm with a time step of 1.0 fs. The system reached a local energy minimum as determined by the density fluctuation after 5 ns. Then, simulated annealing was performed to ensure that the system was not trapped in a local free energy minimum. To accomplish this, the temperature with a constant pressure (1 atm) was gradually increased up to 600 K at a 1 K/10 ps rate and then an NPT dynamic simulation was run at 600 K for 5 ns. Next, the system was cooled to 300 K at a 1 K/10 ps rate and equilibrated for another 20 ns at 300 K.

2.3. Crosslinking Simulations

Several crosslinking algorithms have been established previously for MD simulations, typically based on the close contact criteria, which is commonly employed for amine/epoxy systems to create the complex 3-D crosslinked polymer network.[14-19] Here, we adopt the multi-step crosslinking method developed by Jang *et al*.[20] In that method, a covalent bond between epoxy and amine reactive pairs is formed when two reactive atoms are within the predefined initial search radius of 9.5 Å. Note that each atom has its own search sphere with the same radius. Figure *S*2 shows a schematic 1-D model for this search criterion. Once cross-linking is completed within a particular search radius, the resultant crosslink bonds were fully relaxed through a cycle of relaxation involving every minimization, NVT, and NPT simulations. The search radius was increased by 2 Å when reactive pairs no longer exist at the current search criterion. The maximum

search radius was limited to half the box length which was necessary in order to obey the minimum-image convention rule.

The crosslinking algorithm generally consists of primary amine-epoxy (R''-NH_2 and H_2C-R) and secondary amine-epoxy (R'-NH and H_2C-R) reactions as shown in Figure *S*3 while etherification reactions (R'''-OH and H_2C-R) are typically ignored. Reaction rates for primary amine-epoxy and secondary amine-epoxy reactions are much greater than that for etherification reactions. Furthermore, etherification occurs predominantly in the presence of excess epoxy groups and catalysts such as a tertiary amine at the later stage of curing or at a high temperature cure ~350 °F.[21-25] Therefore, etherification reactions are mainly found in hardener poor systems, especially $r < 0.8$, or after post-curing at a high temperature over 350 °F. We will study the effect of etherification reactions on material properties in future work. Because primary amine reactivity is much greater than secondary amine reactivity, secondary amine reactions were included after most of the primary amines had been depleted. The reactions in the simulation were thus controlled by chemical kinetics and diffusion.

It was necessary to define an upper limit for the degree of crosslinking. The smaller quantity of counter monomers, either epoxy or hardener, was allowed to be completely consumed except for $r = 1.0$. For example, all the amine functional groups for the hardener poor systems r = 0.3, 0.5, and 0.8 were fully reacted and all the epoxy functional groups for the hardener rich systems r = 1.5, 2.0, 2.5, and 3.0 were completely consumed during polymerization. We found, however, that the $r = 1.0$ system had a substantial number of unphysical covalent bond length (e.g., C-N ≥ 3Å) at 100 % crosslinking which could not be relaxed, even after 50 ns NPT equilibration, to the equilibrium bond lengths (r_0 (C-N) < 2.0 Å). Therefore, we redefined the crosslinking limit to 95% for the $r = 1.0$ system. Unphysical bonds create stress accumulation in the system, which

is difficult to release. Thus, the material response to deformation will be predominantly affected by those bonds. The long covalent bonds completely disappeared in the crosslinked structures using the 95% crosslinking limit. Figure 2, for example, shows the bond length distribution of r = 0.8 and r = 1.0 with this criterion. All the bond lengths are simultaneously plotted here. The bond length distributions for the other systems are provided in Figure *S*4.

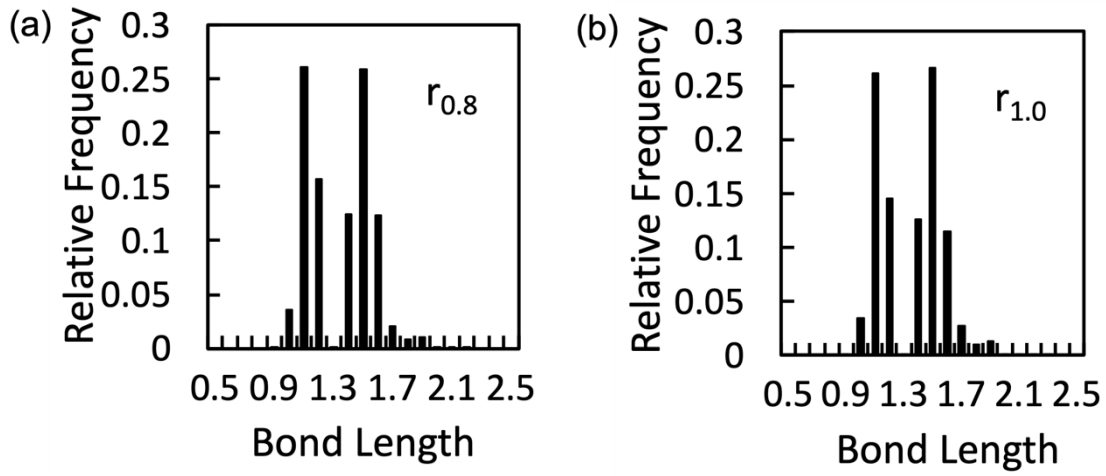

Figure 2. The bond length distribution after equilibration. All the bonds in the crosslinked structures of (a) r = 0.8 and (b) r = 1.0 systems fall within the range of 1 to 2 Å.

Once crosslinking was completed, the system underwent another cycle of equilibration involving geometry optimization, NVT, and NPT simulations to relax the structure and to release any stress induced during crosslinking. The global pairwise cutoff distance was set to 9.5 Å. Simulated annealing simulations from 300 K to 600 K for 10 ns were performed at a rate at 1 K/5 ps. After that, the system was equilibrated for 30 ns at 600 K. The system was then cooled to 300 K and re-equilibrated for 30 ns at 300 K. In this way, each system obtained an equilibrium density in close agreement with the experimental density (in-house experimental densities: 1.292 g/cm^3 for r = 1.0, 1.290 g/cm^3 for r = 0.8, which are less than 5% in difference on average). Topological

update for angles and dihedrals was then carried out with a VMD plugin TopoTools[26] and AmberTools.[27,28] The partial charges were computed from the AM1-BCC model using the Antechamber program.[27-28] Most of the offset models reached their crosslinking limit below the search radius 20 Å.

2.4. Uniaxial Tension Simulation

Stress-strain curves were obtained using a stepwise deformation method in the uniaxial directions (x, y, and z) at several constant strain rates from 10^6 to 10^9 s^{-1} using the "*fix deform*" command in LAMMPS.[12] Young's modulus (E) was measured from the slope in the linear elastic region of the curve. Each Young's modulus was averaged over 15 runs from five systems tested in all directions. The lateral dimension was controlled by the NPT ensemble at 300 K and 1 atm. In this study, we do not consider plastic deformation like strain softening and hardening behaviors. Since gaff2 is a non-reactive force field, it does not include the correct bond breaking which occurs after the yielding. Therefore, we focused on elastic deformation which can be reliably studied with classical force fields.

2.5. Radius of Gyration - R_g

The radius of gyration (R_g) is often used to estimate the size of molecular systems. The radius of gyration of a crosslinked network can be computed at a given time from the moment of inertia I_{system} of the network and the moment of inertia I_{point} of point mass defined as:

$$R_g = \sqrt{\frac{1}{M}\sum_i m_i(r_i - r_{cm})^2} \tag{3}$$

where M and m_i are the total system mass and individual atom mass and r_i and r_{cm} are the positions of the individual atom and the center of mass of the system, respectively. In this study,

we used R_g to describe the degree of rigidity of the crosslinked offset systems. Temperature gradually increased from 300 K to 600 K, and then the expansion coefficient of R_g was measured in the glassy region. Note that this does not give the volume expansion coefficient but rather the expansion coefficient for R_g of the network structure. Therefore, we can determine how much rigid the network structure is upon the mixing ratio *r*.

2.6. Mean Square Displacement

The mean square displacement (MSD) is a measure of the average distance of a group of atoms with respect to a reference position over time. The MSD is defined as

$$MSD =< (x(t) - x_0)^2 >= \frac{1}{N}\sum_{n=1}^{N}(x_n(t) - x_n(0))^2 \quad (4)$$

where $x_n(t)$is the position of each particle at time *t* and $x_n(0)$is the reference position of each particle. If the particles move diffusively, then the MSD curve is linear; however, if particle motion is restricted, the MSD will reach a plateau. So, we can describe molecular flexibility in the crosslinked systems.

2.7. Validation of the model study by experimental measurement

2.7.1. Resin preparation and curing condition

Five compositions of epoxy resin (*r*=0.5, 0.8, 1.0, 1.5 and 2.0) were prepared with API-60 resin and DDS hardener to compare with the MD simulation. The predetermined amount of API-60 resin and DDS mixture were heated to 100°C and mixed for two minutes followed by defoaming for one minute using a planetary mixer. The mixed resin was placed in a mold and degassed in a vacuum oven at 95°C until it stopped bubbling, which took about 30-40 minutes.

The mixed resin was cured in air under ambient pressure for 100°C for 1 hour, 120°C for 1 hour, 140°C for 1 hour, 160°C for 1 hour and 177°C for 3 hours. The heating rate was 3°C/min.\

2.7.2. Density measurement

The density of uncured resin was measured using a volumetric flask. The uncured resin was transferred into a 25 ml volumetric flask with known weight. It took about 20 minutes for the resin to flow into the flask at the elevated temperature of about 90°C. The flask with the resin was weighed and the weight of the resin was calculated. Using a second container, the flask was then filled up to 25 ml mark with water and the weight of water added was measured using the difference in weight of the second container. The volume of water added was calculated using the density of water (1 g/ml). The volume of resin was calculated by subtracting the volume of water added from 25 ml. The density of resin was then calculated from the measured weight and the volume.

The density of cured resin was measured using buoyancy. Four specimens of each resin composition were weighed, and this was recorded as the dry weight. The specimens were suspended in a wire basket in deionized (DI) water and weighed. The suspended weight was subtracted from the dry weight to find the volume of water displaced by the volume of the specimen. The density was calculated from the dry weight and the volume.

2.7.3. Degree of reaction of epoxy and amine, and crosslinking density measurement

Degree of reaction of epoxy and amine, and crosslinking density were analyzed by a Fourier-Transform Infrared (FT-IR) spectroscopy. The infrared (IR) spectra of API-60 resin, DDS and cured resin samples with various ratio of *r* were taken in absorbance mode with a FT-IR spectrometer (Nicolet iS^{TM}-5). Figure *S*5 shows the IR spectra of samples. API-60 epoxy resin

exhibited strong aromatic C-C stretch absorption bands at 1514, 1593 and 1613 cm^{-1} and the absorption band at 1593 cm^{-1} was selected as an internal reference. It also showed a clear oxirane, C-O stretch absorption band which is characteristic peak of uncured epoxy functional group at 907 cm^{-1}. DDS amine hardener exhibited primary amine C-N stretch absorption band at 1274 cm^{-1} and aromatic C-C stretch absorption bands at 1494, 1587 and 1625 cm^{-1}. Degree of reaction of epoxy, degree of reaction of amine (primary) and crosslinking density were calculated from the absorption band areas according to the following equations (5-7):

$$\text{Degree of Reaction of Epoxy} = \frac{Total\ epoxies - Unreacted\ epoxies}{Total\ epoxies}$$

$$= \frac{A_{907cm^{-1}}^{API60} - A_{907cm^{-1}}^{API60-DDS}}{A_{907cm^{-1}}^{API60}} \quad (5)$$

$$\text{Degree of Reaction of Amine} = \frac{Total\ amines - Unreacted\ amines}{Total\ amines}$$

$$= \frac{A_{1274cm^{-1}}^{DDS} - A_{1274cm^{-1}}^{API60-DDS}}{A_{1274cm^{-1}}^{DDS}} \quad (6)$$

$$\text{Crosslinking Density} = \frac{Reacted\ epoxies + Reacted\ amines}{Total\ epoxies + amines}$$

$$= \frac{\left(A_{907cm^{-1}}^{API60} - A_{907cm^{-1}}^{API60-DDS}\right) + \left(A_{1274cm^{-1}}^{DDS} - A_{1274cm^{-1}}^{API60-DDS}\right)}{\left(A_{907cm^{-1}}^{API60} + A_{1274cm^{-1}}^{DDS}\right)} \quad (7)$$

The peak area was normalized by the internal references of aromatic bands and weight fractions of monomers (*r*-values and 15% additive).

2.7.4. Young's modulus measurement

Cured epoxy resins in different offset ratio of *r* were analyzed at different strain frequency by a dynamic mechanical analysis (DMA, Q800, TA Instruments) at 300 K. A tensile clamp fixture was utilized. The sinusoidal tensile strain of 0.1% which resides within the elastic response region of test material was applied. Storage (*E'*) and loss modulus (*E''*) were measured at different strain frequencies of 0.1, 0.32, 1, 3.2, 10, and 31.6 s^{-1} (or Hz). The measured phase shift (tan δ) was as small as 0.01 and the storage modulus representing elastic component of mechanic response was selected to investigate the elastic modulus of cured epoxy systems.[29]

3. RESULTS AND DISCUSSION

3.1. Density and Molecular Packing-volume shrinkage

The performance and properties of epoxy polymer materials can be tuned by altering their microscopic structures, including the degree of crosslinking, the formation of free volume and chain ends, hydrogen bonding, intra-molecular connectivity, and the size and number of clusters.[30-36] Volume shrinkage, which occurs when a liquid epoxy resin is cured into a solid, results from crosslinking. Volume shrinkage was calculated as a function of offset ratio *r* after the crosslinked system was fully equilibrated. Average computed density and volume shrinkage values for each ratio are compared with the experimental values and are given in Figure 3 and Tables *S*2 and *S*3.

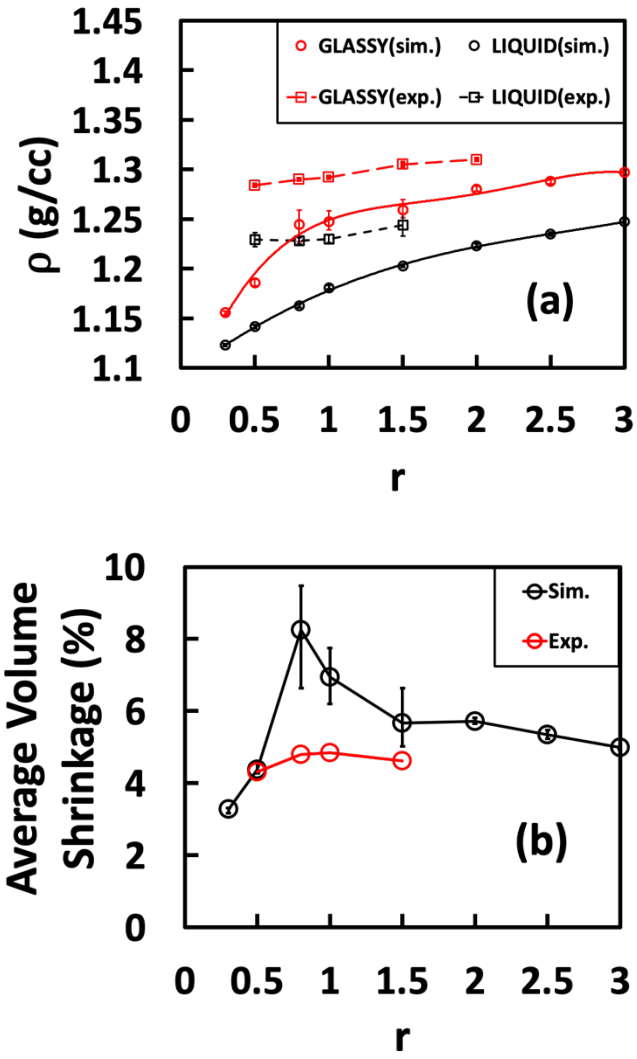

Figure 3. (a) Average mass density, ρ and (b) volume shrinkage as a function of the offset resin from simulations and experiments.

In the uncured liquid state, increasing the amount of hardener enhanced the mass density from about 1.12 to 1.24 g/cm^3. If an excessive amount of hardener were added to the system ($r >> 1$), the density would approach that of the pure hardener. On the other hand, the cured solid systems showed a sharp increase in volume shrinkage close to the mixture $r = 0.8$, resulting in the maximum volume change of $r = 0.8 \sim 1.0$ on average. This indicates that the initial density in the uncured

liquid state was directly proportional to the amount of hardener. After the system became crosslinked, on the other hand, molecular packing is impacted not only by intra-molecular interactions, especially bond/angle interactions, but also by hydrogen bonds from the hydroxyl groups (R-OH). The degree of crosslinking is largest when the mixture is stoichiometrically equivalent, which will be discussed in the section 3.4. The experimental densities of uncured and cured resins were measured as shown in Figure 3(a) and Table *S*3. The densities of both uncured resin and cured resin gradually increased as a function of *r* value, showing similar trend with the MD simulation result. The overall experimental densities were slightly higher than the calculated values with about 3 to 7% difference. This would be caused by the undisclosed toughener in the proprietary API-60 epoxy, which was not included in the simulations. The uncured resin of $r = 2$ exhibited a phase separation of monomers and it was excluded in this study. The volume shrinkage measured from the experiments also showed the similar trend with the MD simulation showing a maximum at around $r = 0.8\sim1.0$ (Figure 3(b) and Tables *S*2 and *S*3). Volume shrinkage influences mechanical property because of the increase in the number of covalent bonds. These bonds restrict segmental motion of the network, thereby increasing the stiffness of the system.

3.2. Mechanical Properties

Uniaxial tension simulations were performed to obtain the Young's modulus using four different strain rates. In general, strain rates used in atomistic simulations are much higher than in the laboratory. The Young's modulus was estimated as the slope of the stress-strain curve as shown in Figure *S*6. Figure 4(a) shows the Young's modulus as a function of mixing ratio *r* by extrapolating simulation results using different strain rates. From line fitting, the semi-log plot was described by coefficients *a* and *b* as shown in Figure *S*7(b). The predicted experimental values of

Young's modulus at the strain rate 10^2 s^{-1} are listed in Table *S*4. All the simulation results are given in Figure *S*7.

$$b = y(x) - aln(x) \tag{8}$$

where y is the computed Young's modulus as a function of strain rate x, a is the slope of simulations results, and b is the predicted Young's modulus at 10^2 s^{-1} strain rate to compare an experimental result.

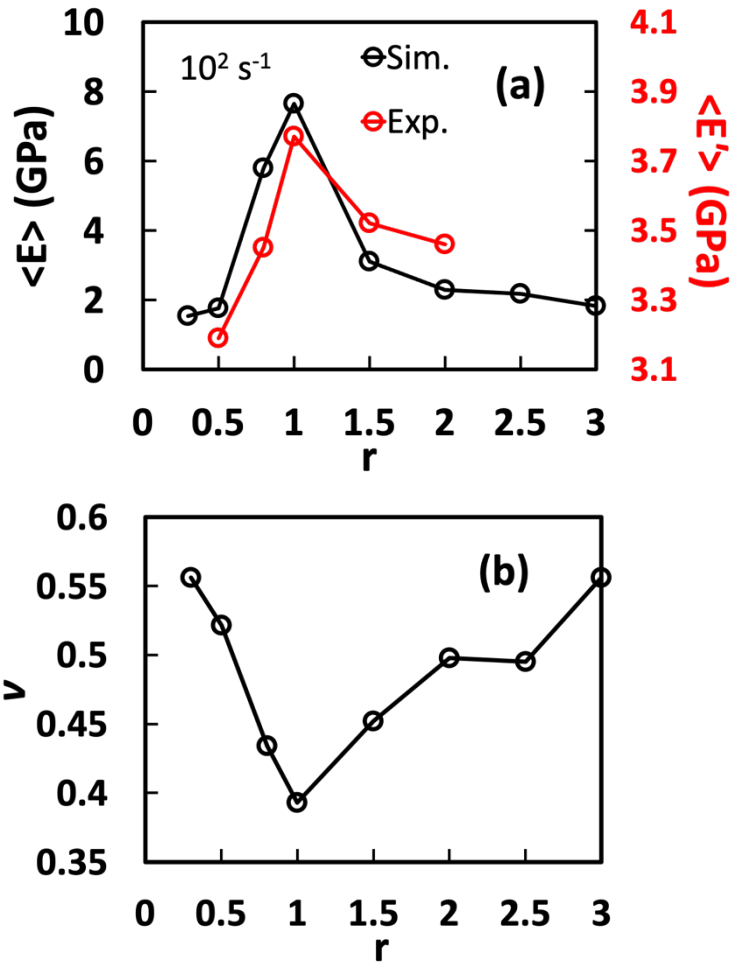

Figure 4. (a) Average computed Young's modulus (E) and measured elastic modulus (E') and (b) average computed Poisson's ratio as a function of r at the strain rate 10^2 s^{-1}. These values resulted from extrapolating values computed at several high strain rates from 10^6 to 10^9 s^{-1} (See Fig. S7(b)).

Young's modulus is sensitive to both offset ratio and strain rate. The maximum Young's modulus was at r = 1.0 and decreased if the offset ratio was asymmetric. The r = 1.0 simulated resin gave a modulus of 10.98 GPa at the strain rate 10^9 s^{-1}, however, extrapolating to low rate gave 7.64 GPa at 10^2 s^{-1}. Modulus values for the mixture TGDDM/TGAP/DDS has not been previously reported. However, the TGDDM/DDS systems have computed elastic modulus of 4~7

GPa reported.[37, 38] Experimental elastic moduli of the cured resins were analyzed using a DMA at different strain frequency of 0.1, 0.32, 1, 3.2, 10 and 31.6 s^{-1} (*S*7(c-d) and Table *S*5) and tensile modulus at the strain rate 10^2 s^{-1} (Figure *S*7(d)) was predicted after extrapolating the results to compare simulation result. The experimental strain rate was much lower than the MD simulation condition due to the limit of the test machine. However, the trend of measured elastic modulus was similar to that of the simulation result, showing a maximum modulus of about 3.4 GPa at r = 1.0 (Figure 4(a)) at the strain frequency of 1 s^{-1}, and decreasing as farther away from the stoichiometric condition. The moduli of r = 0.5 and r = 2.0 were about 2.95 GPa and 3.10 GPa, respectively at the strain frequency of 1 s^{-1}. The effect of strain frequency on the experimental elastic modulus showed the similar trend with the MD simulation (Figures *S*7 (c-d)). As the strain frequencies increased, the elastic modulus increased. The discrepancy between absolute values of experimental and simulation results seems to be originated from the different strain rate, sinusoidal strain of DMA and the uncertainty of components of API-60 epoxy resin. Note also that each MD epoxy model is the ideal case of an experimental design with no void and defect sites, whereas experimental cured epoxy samples could contain them. This could overestimate stiffness in the simulation. We have already evaluated the effect of voids on the elastic/plastic properties and observed more accurate result of the stiffness when we developed a force field and contained an explicit void in an epoxy model. We will discuss this in the future.

Poisson's ratio is another important physico-mechanical property that characterizes the volume compressibility of a material during deformation. The fraction of lateral strain versus longitudinal strain gives the computed Poisson's ratio as shown in Figure 4(b) and Figure *S*8 and is given as:

$$\upsilon = -\frac{0.5\left(d\varepsilon_j + d\varepsilon_k\right)}{d\varepsilon_i} \tag{9}$$

where υ is Poisson's ratio, ε_j and ε_k are lateral strains perpendicular to the tensile direction, and $\varepsilon_i$is longitudinal strain parallel to the tensile direction (x, y, or z). From the results shown in Figure 4(b) and Figure *S*8, the Poisson's ratio depends on both the offset ratio and strain rate. The predicted Poisson's ratio values follow the trend of Young's modulus. Poisson's ratio decreased as the system approached r = 1.0. In general, stiffer materials (higher Young's modulus) require more energy to displace chain segments in the network structure. The lateral dimension of the r = 1.0 crosslinked system, for example, shrinks more slowly in comparison with other systems. This is because the rotational and translation motion of chain segments in the crosslinked structure are restricted by the high degree of connectivity (Figures 5–8 as shown in the section 3.3). Thus, the r = 1.0 system has the lowest Poisson's ratio. The finding of decreasing Poisson ratio with approaching r = 1 (or increasing degree of cure) is consistent with prior literature. Saseendran *et al*.[39] found that the Poisson ratio of epoxy decreased with increasing degree of cure.

On the other hand, the predicted Poisson's ratio increased with decreasing strain rate. Polymer materials are typically affected by the strain rates. Several studies have reported the effect of strain rate on Poisson's ratio. Sahputra and Echtermeyer[40] studied the effects of temperature and strain rate on the deformation of amorphous polyethylene using molecular dynamics simulations. They found that the Poisson's ratio increased as the strain rate decreased. Nitta and Yamana[41] performed tensile deformation simulation in crystalline polymers and evaluated Poisson's ratios over a wide range of strain rates. They measured Poisson's ratios from necked and unnecked regions and found that the Poisson's ratios of HDPE in the necked region decreased but in the unnecked region increased as the strain rate decreased. In the case of LDPE, the Poisson's ratio increased as the strain rate decreased. However, the Poisson's ratio can be modified by including reinforcements in polymers. Okoli and Smith[42] characterized the effect of strain rate on the

Poisson's ratio of glass/epoxy composites and demonstrated Poisson's ratio was not sensitive to the strain rate due to the presence of fibers in the composites.

3.3. Intramolecular connectivity – Monomer Branching

The highest Young's modulus is found for $r = 1.0$. In general, values of Young's modulus depend upon the amount of hardener. The stiffness of a network polymer is mainly affected by crosslinking which is determined by the connectivity of the molecules. The network structures of the off-set polymers were analyzed by enumerating functional groups as either reacted or unreacted. The reacted epoxy and hardener molecules were first classified according to the monomer configuration as shown in Figure 5. A tetra-functional epoxy, for example, has five monomer configurations depending on whether the four functional groups are reacted or not. The hardener was classified into primary, secondary, and tertiary amines. We denote each configuration by the number of reacted functional groups. In Figures 6(a) and 6(b), the results show that the number of fully reacted epoxy monomers reached a maximum at $r = 1.0$, indicating that more than 80 % of the epoxy monomers are fully connected in the network while only about 2% of epoxy monomers were fully reacted at $r = 0.3$. For the hardener rich resins $r > 1$, as shown in Figure 6(c), the $r = 2.5$ and $r = 3.0$ systems do not have any single tertiary amine. The large amounts of uncured chain ends from primary and secondary amines make the systems more flexible. On the other hand, the number of tertiary amines sharply increased at $r = 0.8$ and are maximized at $r = 1.0$, leading to a tighter and stiffer network structure. The experimental degrees of reaction of epoxy and amine (primary) were investigated by a FT-IR spectroscopy as shown in Figure *S*5 and Table *S*6. When $r = 1.0$ and 1.5, the epoxy monomers were almost fully reacted (94 ~96%), while the epoxy rich resin ($r = 0.5$) showed only about 70% reaction. About 90% of epoxy was reacted at $r = 2.0$ (hardener rich system). The primary amines of hardener were almost fully reacted for $r = 0.5 \sim 1.5$,

while the hardener rich resin (r = 2.0) exhibited about 80% reaction. Overall trend of degree of reaction of epoxy and amine was similar to that of the MD simulation, but the experimental degree of reaction at r <1 or >1 was slightly higher than the simulation result. The difference seems to be originated from the uncertainty of components of API-60 epoxy resin (company proprietary toughener) and the etherification reaction during the curing process.

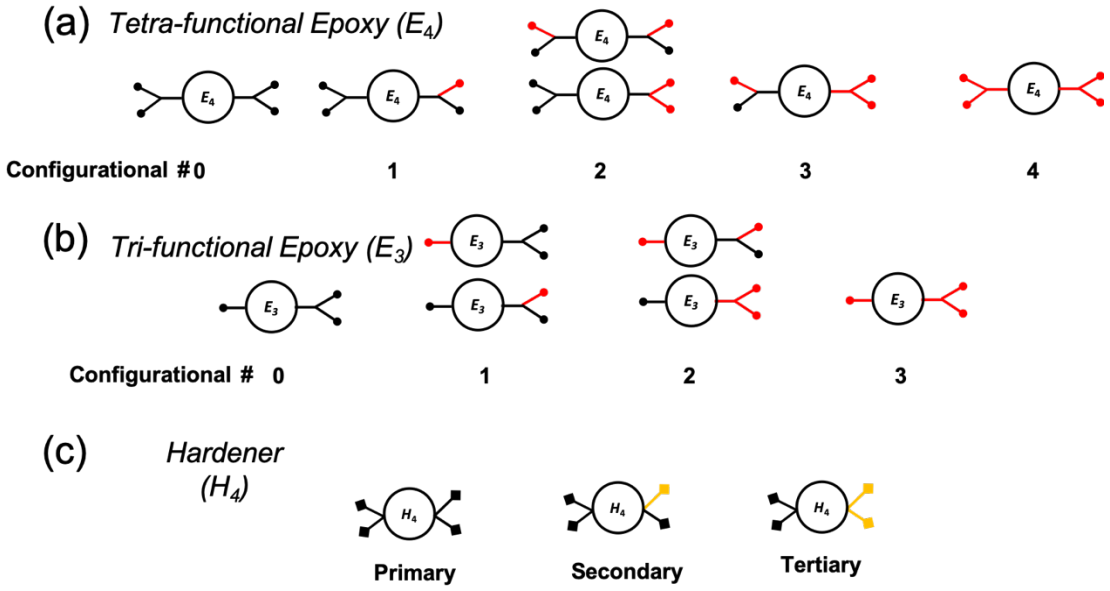

Figure 5. Monomer configuration according to the connectivity. (a) Tetra-functional and (b) Tri-functional epoxies from no reactive functional to fully reacted functionals. (c) Tetra-functional hardener configuration model. Color represents the reacted functional ends in red and yellow.

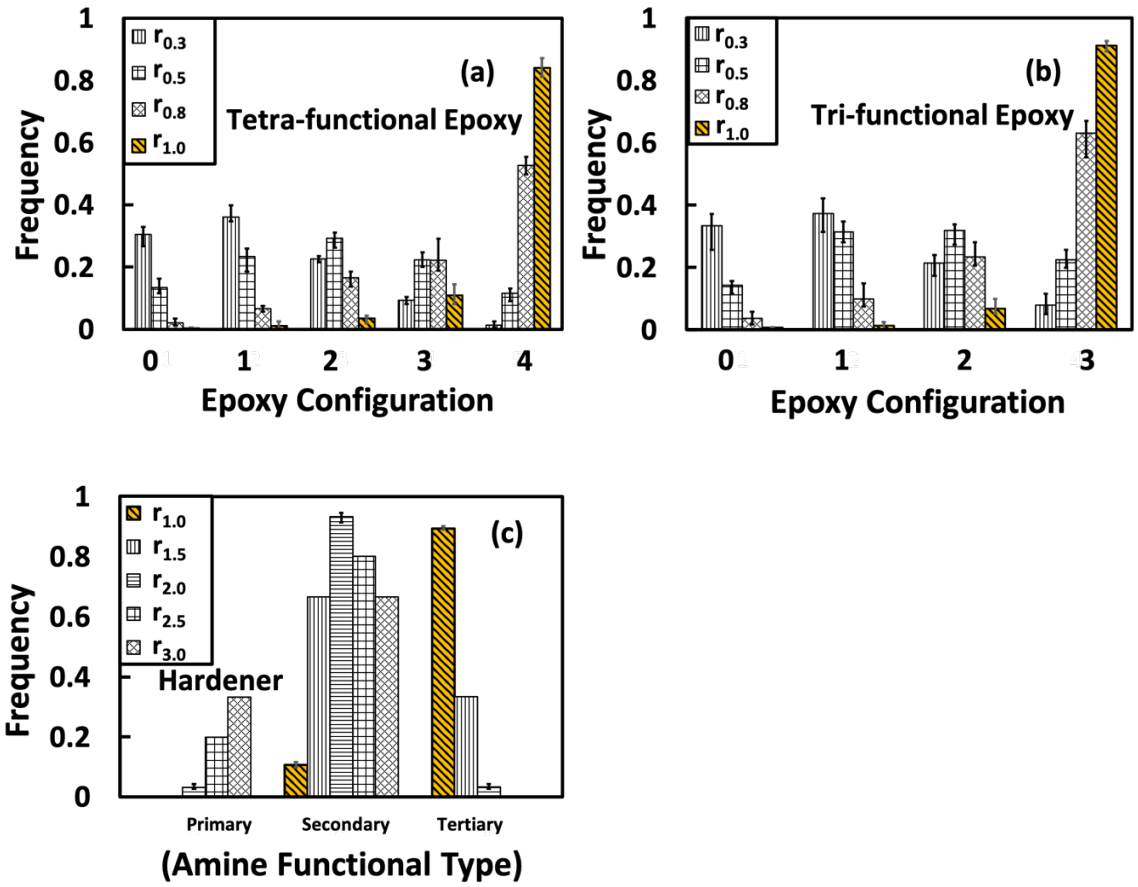

Figure 6. The fractional number of (a) (b) epoxy monomers and (c) hardener to the connectivity configuration. The yellow bar for r = 1.0 is indicated for reference.

3.4. Clustering Analysis

3.4.1. Cluster Distribution

The polymer molecules are linked together and become a percolating network cluster as the degree of crosslinking increases. After the system was fully cured, the number of clusters and the largest cluster size were determined. The cluster here is defined as when at least two molecules are connected. The smallest cluster, therefore, is a single epoxy molecule and single hardener molecule. It is evident in Figure 7 that the offset ratio affected the number and size of clusters. Almost all the

molecules on average were assembled into a single cluster only at r = 1.0. For non-stoichiometric r values, the system is more fragmented. This is clearer in Figure 8 where the largest cluster at r = 1.0 has 100% of the molecular weight of the system. Note that only the r = 1.0 system absorbed all the molecules into a single cluster. Whereas, all other systems have some remaining monomers or at least one smallest cluster (single epoxy + single hardener) as shown in the Figure 7(a) inset. The system at r = 0.8 does not contain any small clusters but does have some uncured monomers. However, the system at r = 1.5 has small clusters like two- or three-monomers' clusters with no intact monomers remaining. Increasing the degree of crosslinking severely restricts the polymer chain segmental mobility and determines, to a great extent, the crosslinked system properties. The experimental crosslinking density measured by FT-IR analysis validated the trend of the simulated crosslinking density as shown in Figure 8 and Table *S*6. The system at r = 1.0 showed over 97% crosslinking density while the system at r = 0.5 (epoxy rich) or 2.0 (hardener rich) showed lower crosslinking density of about 85 ~ 87%. In particular, cluster analysis allows one to understand the change of the stiffness of the system, as reflected by the results of Young's modulus.

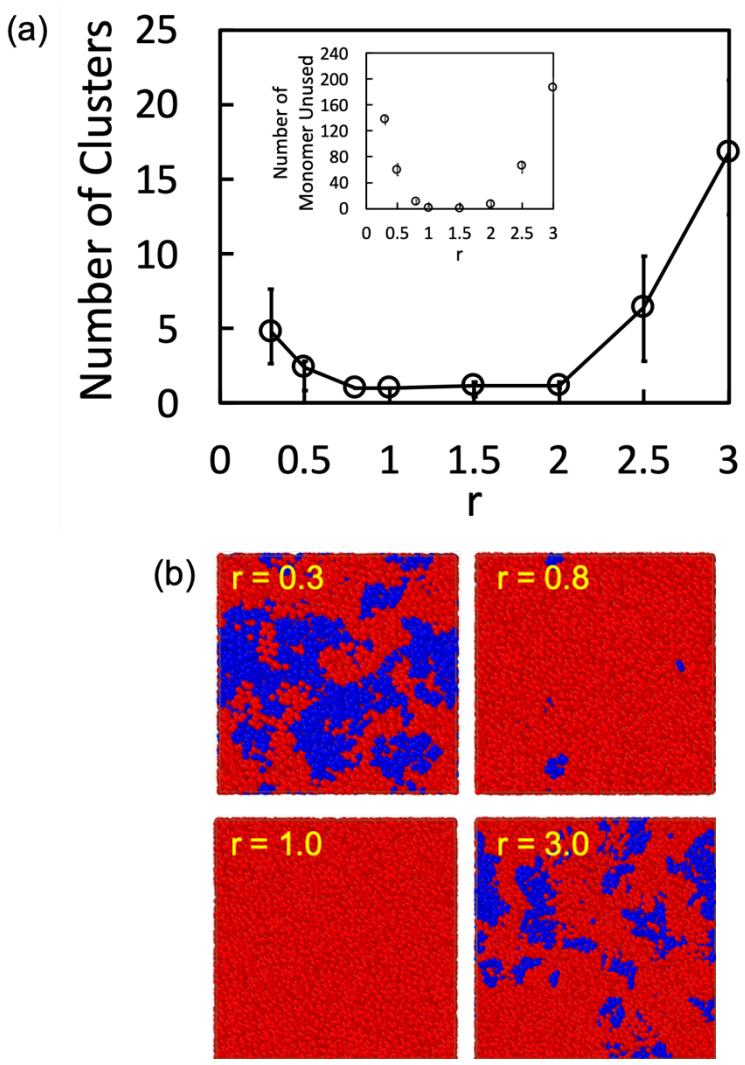

Figure 7. Top: The fraction of clusters as a function of *r*. An inset plot is the number of intact monomers which does not have a single link to any clusters. Bottom: The simulation snap shots for crosslinked offset polymers. (red: the largest network cluster, blue: uncured monomers and small clusters)

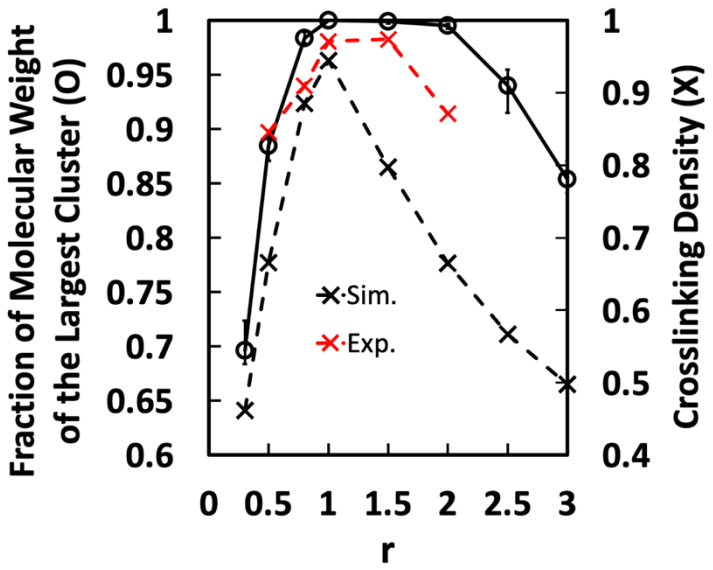

Figure 8. The weight fraction of the largest cluster (solid line) and degree of crosslinking (dashed line) corresponding to *r*. Experimental crosslinking density (red dashed line) was measured by FT-IR spectroscopy.

3.4.2. Connection between stiffness and thermal expansion

In general, thermal expansion and stiffness are inversely related. We considered the effect of thermal strain on the radius of gyration which can reveal the dependence of the network cluster conformation on stiffness. Temperature was slowly increased from 300 K to 600 K causing the radius of gyration of the largest cluster to expand as shown in Figure 9. The temperature-dependent radius of gyration ($\frac{\Delta R_g}{\Delta T}$) is low when stiffness is high and vice versa. The r = 0.3 system was considerably more sensitive to thermal strain whereas the r = 1.0 system exhibited less sensitivity to temperature change. Lowest expansion at r = 1.0 indicates that strong inter- and intra-molecular forces are needed to restore the network structure when the molecules are pulled apart. The largest network cluster in the r = 1.0 system (indeed, there is only one cluster in the r = 1.0 system, see

Figure 7) was insensitive to thermal strain while the offset systems showed greater expansion due to the reduced stiffness.

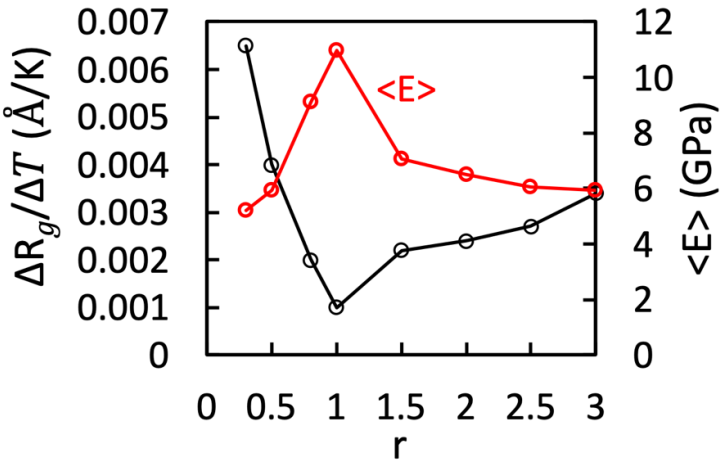

Figure 9. The relation between the computed Young's modulus and thermal expansion measured at the 10^9 s^{-1} strain rate.

3.4.3. MSD of the Largest Cluster

The chain segments in a network structure do not freely move but are constrained. The MSD for the network structure linearly increases due to the small vibrational motion of atoms, however, it reaches a plateau as shown in Figure *S*9 because of the network constraints which restrict further movement. The trajectories of particles were recorded and analyzed in terms of MSD in order to determine the relative flexibility of the offset systems. As illustrated in Figure 10, all the systems showed the typical behavior of a constrained network polymer. The average displacement of particles in the network can be measured by the value of the plateau. The $r = 1.0$ system, as expected, showed less diffusion because most of the particles were strongly connected and thus constrained by the network (see Figure 7). As a result, epoxy rich resin system ($r < 1$) had larger diffusivity because the epoxy molecules, which were unreacted or loosely crosslinked, were

more flexible than the stiff hardener molecules (two phenyl rings terminated with short amine groups) in the hardener rich resin systems ($r > 1$). We must bear in mind that etherification reactions should be considered for epoxy rich systems ($r < 1$), as they might affect the material characteristics. This effect will be discussed in future work.

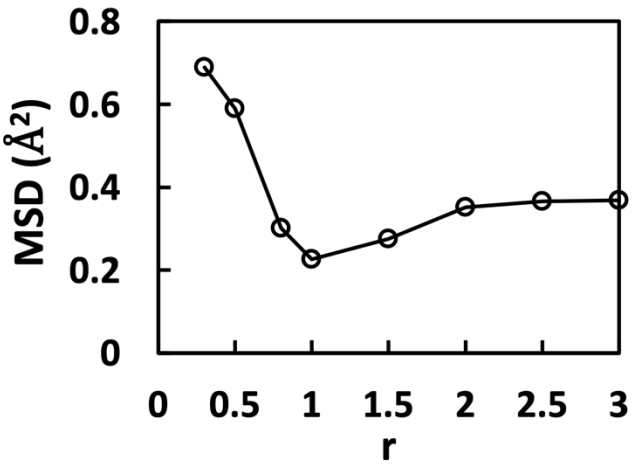

Figure 10. The MSD shows that the $r = 1.0$ system is most constrained. It also represents the degree of rigidity as a function of r. The results were obtained from the MSD plateau values.

4. CONCLUSIONS

In this work, the structural and mechanical properties of an off-stoichiometric epoxy/amine resin were considered. These resins are of interest for adhesive-free, reflowable-interface bonding techniques for composite structures. Atomistic molecular dynamics (MD) simulations were performed to understand structure-property relationship in these systems. The co-cure-ply method is an advanced method to assemble the large-scale aerospace composite structure. In this method, the resin is cured in a two-step curing process and produces a strong and reliable bond at the composite-composite interface without the need for additional mechanical fasteners. In the primary cure, the supporting structure is fully cured while the mating surface remains only partially cured due to its stoichiometric offset (e.g., epoxy rich and hardener rich). The complementary

offset stoichiometric surfaces are then mated and cured in a secondary cure cycle. During the secondary cure, the ER/HR interface reflows, mixes, and cures. The interface can be heterogeneous microscopically depending on the hardener/epoxy formulation and the degree of mixing achieved. MD simulations were used to predict the mechanical properties in local domains as a function of hardener/epoxy ratios from $r = 0.3$ to 3.0. These simulations provide a detailed description of the structure-property relationships at the atomistic scale.

Young's modulus was computed from uniaxial tension simulations. We investigated the relationship of the stiffness to crosslinked structural properties such as intra-molecular connectivity, radius of gyration, mean squared displacement, crosslinked density, molecular weight of the largest network cluster and cluster expansion induced by the thermal strain. Young's modulus increased as the stoichiometric ratio approached the stoichiometric hardener/epoxy mixture $r = 1.0$ and decreased as the formulation became more non-stoichiometric ($r < 1$ or $r > 1$). In particular, we found that the crosslinking density and the molecular weight of the largest network cluster were maximized at $r = 1.0$ with dense branching monomer structures. That is, most of reactive functional groups for both epoxies and hardeners were depleted to form the largest cluster at $r = 1.0$ while off-stoichiometric resins ($r \neq 1.0$) had unreacted functional groups present in the largest cluster and pure monomers (see Figures 6 and 7). In fact, unreacted functional groups create chain-end free volumes. These unoccupied spaces allow for more flexible network structures that are better able to absorb strain without transmitting it to the crosslink bonds, thereby reducing internal stress during the deformation.[43-47] The atomistic MD simulations were validated with experimental measurement of density, reaction of monomers, crosslinking density, and modulus. There were some differences between the experimental result and simulations, but they were within reasonable errors.

Full interfacial properties can be estimated using a multi-scale framework, where MD simulations are performed in local *nano-scale* domains. These calculated parameters can then be utilized in higher scale modeling like finite element analysis (FEA) to determine the properties of the full composite interface. Such an approach will be reported in future work.

SUPPORTING INFORMATION

Chemical structures of API-60 epoxy; Number of molecules and molecular weight as a function of the offset ratio; Schematic figure of search criterion; Crosslinking Algorithm; Bond length distribution after cure and equilibration; FT-IR spectra of API60 epoxy; Table for average mass density and volume shrinkage; Table for experimental mass density of uncured and cured resin; MD stress-strain curves; MD and experimental Young's modulus as a function of mixing ratio *r*; Table for computed Young's modulus; Table for measured Young's modulus; Poisson's ratio computed from MD; Table for experimental degree of reaction and crosslinking density; Root mean square displacement of offset systems

AUTHOR INFORMATION

Corresponding Authors
Chang Woon Jang
*E-mail: changwoon.jang@nasa.gov
John W. Lawson
*E-mail: john.w.lawson@nasa.gov

ACKNOWLEDGEMENTS

We acknowledge funding support from the NASA Aeronautic Research Mission Directorate's (ARMD's) Convergent Aeronautic Solutions (CAS) project.

REFERENCES

(1) Mouritz, A. P. Introduction to aerospace materials.; Woodhead Publishing: Cambridge, **2012**; pp 285.

(2) Palmieri, L. P.; Connell, J. W.; Whol, C. J. Off-set resin formulations and blocking/deblocking resin systems for use as a "co-cure-ply" in the fabrication of large-scale composite structure. US 20170368812A1, United States Patent and Trademark Office, 28 December **2017**.

(3) Palmieri, L. P.; Connell, J. W.; Whol, C. J. Off-set resin formulations and blocking/deblocking resin systems for use as a "co-cure-ply" in the fabrication of large-scale composite structure. US 20170368812A1, United States Patent and Trademark Office, 28 December **2017**.

(4) Palmieri, L.P.; Hudson, T. B.; Smith, A. J.; Cano, R. J.; Lin, Y.; Kang, J. H.; Crossett, K. M; Clifford, B.; Connell, J. W. "Epoxy matrix resins with offset stoichiometry for predictable joints in composite assemblies," *American Chemical Society Fall National Meeting & Expo Electronic Proceedings (abstract only, invited talk)*, Virtual Event, August 16-20, **2020**.

(5) Palmieri, L.P.; Hudson, T. B.; Smith, A. J.; Cano, R. J.; Lin, Y.; Kang, J. H.; Crossett, K. M; Clifford, B.; Connell, J. W. "Modified epoxy matrix resins for reduced dependence on redundant fasteners in secondary-bonded composite structures," *SAMPE Technical Conference Proceedings,* Virtual Event (Originally Seattle, WA), June, 2020 and *SAMPE Europe Technical Conference Proceedings*, Virtual Event (Originally Amsterdam, Netherlands), September 30-October 1, **2020**.

(6) Palmieri, L.P.; Hudson, T. B.; Smith, A. J.; Lin, Y.; Kang, J. H.; Crossett, K. M; Clifford, B.; Connell, J. W. "Modified epoxy matrix resins for reduced dependence on redundant fasteners in secondary-bonded composite structures," *American Chemical Society (ACS) Spring National Meeting & Expo Proceedings,* Virtual Event (Originally Philadelphia, PA), March 22-26, **2020**.

(7) Palmieri, L.P.; Hudson, T. B.; Smith, A. J.; Lin, Y.; Kang, J. H.; Crossett, K. M; Clifford, B.; Connell, J. W. "Reduced dependence on redundant fasteners in secondary-bonded composite structures using modified epoxy matrix resins," *43rd Meeting of the Adhesion Society Proceedings,* Charleston, SC, February 23-26, **2020**.

(8) Palmieri, F. L.; Hudson, T. B.; Cano, R. J.; Tastepe, E. R.; Rufeisen, D. S.; Ahmed, L. U.; Lin, Y.; Wohl, C. J.; Connell, J. W. "Reliable bonding of composite laminates using reflowable epoxy resins," *SAMPE Technical Conference Proceedings,* Charlotte, NC, May 20-23, **2019**.

(9) Palmieri, F. L.; Hudson, T. B.; Cano, R. J.; Tastepe, E. R.; Rufeisen, D. S.; Ahmed, L. U.; Wohl, C. J.; Connell, J. W. "Adhesive joining of composite laminates using epoxy resins with stoichiometric offset," *42nd Meeting of the Adhesion Society Proceedings,* Hilton Head, SC, February 17-20, **2019**.

(10) Mohan, J.; Ivanković, A.; Murphy, N. Mode I fracture toughness of co-cured and secondary bonded composite joints. *Int. J. Adhes. Adhes.*, **2014**, 51, 13-22.

(11) Martínez, L.; Andrade, R.; Birgin, E. G.; Martínez. J. M. Packmol: A package for building initial configurations for molecular dynamics simulations. *J. Comput. Chem.*, **2009**, 30(13), 2157-2164.

(12) Plimpton, S. Fast Parallel Algorithms for Short-Range Molecular Dynamics. *J. Comput. Phys.*, **1995**, 117(1), 1-19.

(13) GAFF2 are public domain force fields and are part of the AmberTools19 distribution, available for download at http://amber.org/AmberTools.php (accessed September **2019**).

(14) Komarov, P. V.; Yu-Tsung, C.; Shih-Ming, C.; Khalatur, P. G.; Reineker, P. Highly Cross-Linked Epoxy Resins: An Atomistic Molecular Dynamics Simulation Combined with a Mapping/Reverse Mapping Procedure. *Macromolecules.*, **2007**, 40(22), 8104-8113.

(15) Varshney, V.; Patnaik, S. S.; Roy, A. K.; Farmer, B. L. A Molecular Dynamics Study of Epoxy-Based Networks: Cross-Linking Procedure and Prediction of Molecular and Material Properties. *Macromolecules.*, **2008**, 41(18), 6837-6842.

(16) Li, C.; Strachan. A. Molecular Simulations of Crosslinking Process of Thermosetting Polymers. *Polymer.*, **2010**, 51(25), 6058-6070.

(17) Li, C.; Strachan, A. Molecular Dynamics Predictions of Thermal and Mechanical Properties of Thermoset Polymer EPON862/DETDA. *Polymer.*, **2011**, 52(13), 2920-2928.

(18) Ghosh, S.; Kumar, A.; Sundararaghavan, V.; Waas, A. M. Non-Local Modeling of Epoxy Using an Atomistically-Informed Kernel. *Int. J. Solids. Struct.*, **2013**, 50(19), 2837-2845.

(19) Jang, C.; Lacy, T. E.; Gwaltney, S. R.; Toghinai, H.; Pittman, C. U. Relative Reactivity Volume Criterion for Cross-linking: Application to Vinyl Ester Resin Molecular Dynamics Simulations. *Macromolecules.*, **2012**, 45(11), 4876-4885.

(20) Jang, C. W.; Sirk, T. W.; Andzelm, J. W.; Abrams, C. F. Comparison of Crosslinking Algorithms in Molecular Dynamics Simulation of Thermosetting Polymers. *Macromol. Theory Simul.*, **2015**, 24(3), 260-270.

(21) Mijovic, J.; Wijaya, J. Etherification Reaction in Epoxy-Amine Systems at High Temperature. *Polymer.*, **1994**, 35(12), 2683-2686.

(22) Xu, L.; Schlup, J. R. Etherification versus Amine addition during Epoxy Resin/Amine Cure: An *in situ* study using near-infrared spectroscopy. *J. Appl. Polym. Sci.*, **1998**, 67(5), 895-901.

(23) Vyazovkin, S.; Sbirrazzuoli, N. Mechanism and Kinetics of Epoxy-Amine Cure Studied by Differential Scanning Calorimetry. *Macromolecules.*, **1996**, 29(6), 1867-1873.

(24) Pramanik, M.; Fowler, E. W.; Rawlins, J. W. Cure Kinetics of Several Epoxy-Amine Systems at Ambient and High Temperatures. *J. Coat. Technol. Res.*, **2014**, 11, 143-157.

(25) Hseih, H. K.; Su, C. C.; Woo, E. M. Cure Kinetics and Inter-domain Etherification in an Amine-cured Phenoxy/epoxy System. *Polymer*., **1998**, 39(11), 2175-2183.

(26) Humphrey, W.; Dalke, A.; Schulten, K. VMD - Visual Molecular Dynamics, *J. Molec. Graphics.*, **1996**, 14(1), 33-38.

(27) Wang, J.; Wang, W.; Kollman P. A.; Case, D. A. Automatic Atom Type and Bond Type Perception in Molecular Mechanical Calculations. *J. Mol. Graph. Model.*, **2006**, 25(2), 247260.

(28) Wang, J.; Wolf, R. M.; Caldwell, J. W.; Kollman, P. A.; Case, D. A. Development and testing of a general AMBER force field. *J. Comput. Chem.*, **2004**, 25(9), 1157-1174.

(29) Meyers, M.; Chawla, K. Mechanical Behavior of Materials; 2nd Edition, Cambridge University Press, 2009; pp 124.

(30) Mark, J. E. Mechanical Properties of Polymers Based on Nanostructure and Morphology. Edited by Georg H. Michler and Francisco J. Balta′-Calleja. *Angew. Chem. Int. Ed.*, **2006**, 45, 6080.

(31) Askadskii, A. A. Influence of Crosslinking Density on the Properties of Polymer Networks. *Polym. Sci.* (*USSR*)., **1990**, 32(10), 2061-2069.

(32) Oya, Y.; Kikugaws, G.; Okabe, T. Clustering Approach for Multidisciplinary Optimum Design of Cross-Linked Polymer. *Macromol. Theory Simul.*, **2017**, *26* (2), 1600072.

(33) Gupta, V. B.; Brahatheeswaran, C. Molecular Packing and Free Volume in Crosslinked Epoxy Networks. *Polymer.*, **1991**, 32(10), 1875-1884.

(34) Shen, X.; Liu, X.; Dai, J.; Liu, Y.; Zhang, Y.; Zhu, J. How Does the Hydrogen Bonding Interaction Influence the Properties of Furan-Based Epoxy Resins. *Ind. Eng. Chem. Res.*, **2017**, 56(38), 10929-10938.

(35) Ba, L.; Zou, Q.; Tan, X.; Song, J.; Cheng, J.; Zhang, J. Structure, Morphology and Properties of Epoxy Networks with Dangling Chains Cured by Anhydride. *RSC Adv.*, **2016**, 6(94), 91875-91881.

(36) Nielsen, L. E. Cross-linking-effect on Physical Properties of Polymers. *J. Macromol. Sci. Polymer. Rev.*, **1969**, 3, 69-103.

(37) Foreman, J. P.; Porter, D.; Behzadi, S.; Travis, K. P.; Jones, F. R. Thermodynamic and Mechanical Properties of Amine-cured Epoxy Resins using Group Interaction Modeling. *J. Mater. Sci.*, **2006**, 41(20), 6631-6638.

(38) DiFrancia, C.; Ward, T. C.; Claus, R. O. The Single-fibre Pull-out Test. 2: Quantitative Evaluation of an Uncaltalysed TGDDM/DDS Epoxy Cure Study. *Compos. Part A-Appl S.*, **1996**, 27(8), 613-624.

(39) Saseendran, S.; Wysocki, M.; Varna, J. Cure-state Dependent Viscoelastic Poisson's ratio of LY5052 Epoxy Resin. *AMPCS.*, **2017**, 3(3), 92-100.

(40) Sahputra, I. H.; Echtermeyer, A. T. Effects of Temperature and Strain Rate on the Deformation of Amorphous Polyethylene: A Comparison between Molecular Dynamics Simulations and Experimental Results. *Model. Simul. Mater. Sci. Eng.*, **2013**, 21(6), 065016.

(41) Nitta, K-h.; Yamana, M. Poisson's Ratio and Mechanical Nonlinearity under Tensile Deformation in Crystalline Polymers. In: De Vicente J (ed) Rheology. InTech. ISBN 978-953-51-0187-1. https://www.intechopen.com/books/rheology/poisson-s-ratio-and-mechanical-nonlinearity-under-tensile-deformation.

(42) Okoli, O. I.; Smith, G. F. The Effect of Strain Rate and Fibre Content on the Poisson's ratio of Glass/Epoxy Composites. *Compos. Struct.*, **2000**, 48(1-3), 157-161.

(43) Li, Chunyu.; and Strachan, A. Free Volume Evolution in the Process of Epoxy Curing and Its Effect on Mechanical Properties. *Polymer.*, **2016**, 97(5), 456-464.

(44) Altaweel, A. M. A. M.; Ravikumar, H. B.; Ranganathaiah, C. Influence of Free Volume on the Mechanical Properties of Epoxy based Composites: A Correlation Study. *Phys. Status Solidi C.*, **2009**, 6(11), 2401-2403.

(45) Huang, Y.; Tian, Y.; Li, Y.; Tan, X.; Li, Q.; Cheng, J.; Zhang, J. High Mechanical Properties of Epoxy Networks with Dangling Chains and Tunable Microphase Separation Structure. *RSC Adv.*, **2017**, 7(77), 49074.

(46) Nograro, F. F. d.; Llano-Ponte, R.; Mondragon, I. Dynamic and Mechanical Properties of Epoxy Networks Obtained with PPO based Amines/mPDA Mixed Curing Agents. *Polymer.*, **1996**, 37(9), 1589-1600.

(47) Li, J.; Wu, Z.; Huang, C.; Huang, R.; Li, L. Mechanical Behaviors of Hyberbranched Epoxy Toughened Bisphenol F Epoxy Resin for Cryogenic Applications. *AIP Conf. Proc.*, **2014**, 1574, 125-131.